Computational Materials Science 249 (2025) 113641

Contents lists available at ScienceDirect

Computational Materials Science

journal homepage: www.elsevier.com/locate/commatsci

Full length article

Deep-neural-network molecular dynamics investigation of phonon thermal transport in polyether ether ketone

Haoran Cui, Weijian Hua, Lei Cao, Yifei Jin *, Yan Wang *

Department of Mechanical Engineering, University of Nevada, Reno, Reno, 89557, NV, USA

ARTICLE INFO

Keywords:
Thermal conductivity
Polymer
Amorphous
Phonon
Polyether ether ketone

ABSTRACT

Polyether ether ketone (PEEK) is an important high-performance engineering thermoplastic, yet the thermal transport properties of its crystalline and single-chain forms remain elusive. In this work, a deep neural network interatomic potential is trained using ab initio molecular dynamics to accurately model thermal transport in bulk crystalline, bulk amorphous, and single-chain PEEK. Additionally, phonon thermal transport across chains, which are grouped together through van der Waals (vdW) interactions, exhibits a weak dependence of thermal conductivity (κ) on the number of chains, i.e., weakly ballistic transport in cross-chain directions. This behavior contrasts with many layered materials bonded by vdW interactions, which often show a strong dependence of cross-plane κ on the number of layers. This work facilitates the understanding of thermal transport properties of PEEK and phonon transport in vdW-bonded materials in general, offering a theoretical guideline for predicting optimal conditions for PEEK processing and beyond.

1. Introduction

Polyether ether ketone (PEEK) is a high-performance engineering thermoplastic that is highly valued in engineering applications due to its exceptional combination of mechanical strength [1,2], chemical resistance [3,4], and thermal stability [5,6]. PEEK exhibits excellent strength and stiffness, making it suitable for demanding structural applications, while its outstanding resistance to a wide range of chemicals ensures longevity and reliability in harsh environments [4]. Notably, PEEK maintains its mechanical integrity at high temperatures, with a continuous application temperature of approximately 250 °C [7,8]; moreover, it also has excellent resistance to radiation or hydrolysis [9,10]. These unique properties render PEEK an ideal material for various applications in the aerospace [11], and automotive industries [12], where durable, lightweight, and high-performance materials are crucial for enhancing efficiency and performance. Its biocompatibility also enables its use in medical implants and devices, further broadening its application scope [13,14]. Consequently, the three-dimensional (3D) printing of PEEK has received significant attention in recent years for manufacturing high-temperature performance components for various applications [15]. However, despite some experimental data, the fundamental thermal transport mechanisms in PEEK remain elusive.

Over the past decade, phonon thermal transport in non-conductive polymers has garnered significant attention, yielding notable insights through experimental and computational studies. It is now well-established that a stand-alone, single-chain polymer can exhibit much higher lattice thermal conductivity (κ) compared to its bulk crystalline counterpart [16,17]. Furthermore, amorphous polymers have much lower κ than their crystalline counterparts due to entangled phonon transport pathways [18]. Thus, understanding the theoretical upper limit of κ for PEEK, specifically that of single-chain PEEK, is of significant importance. To date, all studies on bulk polymers have focused exclusively on thermal transport along the chain direction, mediated by covalent bonds, while phonon transport across polymer chains, mediated by van der Waals (vdW) interactions, has not been investigated. Recent studies on 2D vdW materials have sparked interest in phonon transport across vdW-bonded layers, revealing that κ in the cross-plane direction can significantly depend on the layer count. This finding motivates an investigation into how the number of polymer chains affects κ in the cross-chain direction for PEEK, given that the chains are also bonded through vdW interactions. The obtained knowledge from this work can be directly utilized in the simulation of PEEK 3D printing, especially fused deposition modeling of PEEK, where polymer chains are aligned in a layer-by-layer manner.

2. Methodology

2.1. Deep neural network interatomic potential

Recent advancements in the field have demonstrated that deep neural network (DNN) potentials are significantly more accurate than

* Corresponding authors.
E-mail addresses: yifeij@unr.edu (Y. Jin), yanwang@unr.edu (Y. Wang).

https://doi.org/10.1016/j.commatsci.2024.113641
Received 9 July 2024; Received in revised form 14 December 2024; Accepted 22 December 2024
Available online 1 January 2025

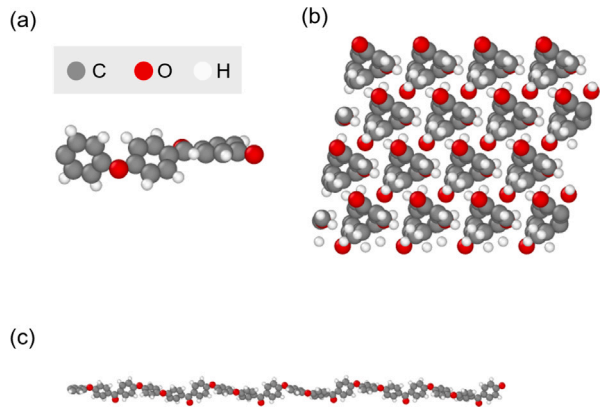

Fig. 1. Schematics of (a) PEEK unit cell, (b) bulk PEEK with a staggered stacking order, and (c) single-chain PEEK. Specifically, C atoms are gray, O atoms are red, and H atoms are white.

conventional explicit-form empirical interatomic potentials [19,20]. Additionally, DNN potentials enable the atomistic modeling of millions of atoms on supercomputers, allowing the accurate calculation of material properties and behaviors that are beyond the capabilities of either molecular dynamics (MD) using conventional potentials which is limited by accuracy [20], or ab initio molecular dynamics (AIMD) which is limited by computational cost [19].

To train a DNN potential, we first conduct extensive AIMD simulations using the Vienna ab initio simulation package (VASP) for bulk PEEK, single-chain PEEK, and PEEK structures with free surfaces or gaps. The unit cell structure of PEEK is displayed in Fig. 1a and the relaxed structures of bulk PEEK and single-chain PEEK are shown in Fig. 1b and c, respectively. In our AIMD simulations, we utilize a Γ-centered scheme to ensure the fast collection of training data on large supercells of PEEK. We employ a plane-wave cut-off energy of 600 eV and a Gaussian smearing width of 0.05 eV, with a convergence threshold of 10^{-7} eV for self-consistent electronic iterations, ensuring precise force calculations. These simulations are performed within the isothermal–isobaric (NPT) ensemble at various temperatures and pressures, ranging from 300 K to 1000 K (well above the melting point of PEEK) and from −1 GPa to 50 GPa, respectively, to capture as many essential states of the system as possible. Additionally, structural minimization calculations within density-functional theory (DFT) are performed on melted or amorphous PEEK, and the resulting data are also used to train our DNN potential.

All AIMD and DFT data, including cell parameters, atomic positions, atomic forces, and energies, are utilized to train a DNN interatomic potential using the DeePMD package [19,20]. In DeePMD, we set the parameters to use the full relative coordinates to construct the descriptor during training. We employ a neighbor list with a cutoff radius of 6.0 Å and a smoothing function cutoff radius of 0.5 Å. The embedding network comprises three hidden layers with 32, 64, and 128 neurons, respectively, while the fitting network consists of three hidden layers, each containing 240 neurons. The DNN is trained for 16 million steps with an initial learning rate of 0.001, which decays to 3.51×10^{-8} by the end of the training process.

Fig. 2a, b, and c present the vibrational density of states (vDOS) of carbon, oxygen, and hydrogen atoms in bulk PEEK at 300 K, as predicted by MD simulations using our DNN potential and by AIMD simulations. The excellent agreement between the vDOS predicted by these two methods highlights the high accuracy of our DNN potential. Additionally, we randomly selected 3000 configurations from our AIMD simulations of bulk PEEK and single-chain PEEK under pressures ranging from −1 GPa to 5 GPa and used our DNN potential to predict their energies and atomic forces. As illustrated in Fig. 2d and e, the predicted energies and forces from AIMD align closely with those from our DNN potential, further validating the reliability of the DNN potential.

It is important to note that AIMD data at high pressures of up to 50 GPa were also incorporated into the training dataset for our DNN potential, even though the thermal transport behavior at such extreme pressures is not explored in this work. As shown in Fig. S1 of the Supplementary Materials, the DNN potential exhibits limited accuracy in predicting forces for configurations under ultrahigh pressures, resulting in noticeable outliers (deviating from the diagonal) in the comparison between AIMD and DNN predictions. Nevertheless, we emphasize that including these high-pressure data is essential for broadening the DNN potential's knowledge domain, enabling it to cover a much wider pressure range. This broader range contributes to maintaining structural stability during melting simulations of PEEK.

2.2. Equilibrium molecular dynamics

We performed MD simulations using the Large-scale Atomic/Molecular Massively Parallel Simulator (LAMMPS) package [21], enhanced with the DeePMD plugin [19] to implement our developed DNN interatomic potential. For bulk PEEK, periodic boundary conditions were applied in all three spatial directions, whereas for single-chain PEEK, periodic boundaries were applied only along the chain direction, with non-periodic boundary conditions used in the cross-chain directions. To account for the small mass of hydrogen atoms (1 g/mol), we employed a small time step of 0.05 fs in the simulations.

At the initial stage of the MD simulations, random velocities were assigned to the atoms according to a Gaussian distribution to achieve an average system temperature of 5 K. Subsequently, two NPT relaxation steps, controlled by the Nosé-Hoover thermostat and barostat [22,23], were performed to equilibrate the structure at the target temperature. In the first NPT step, the system temperature was gradually increased from 5 K to the target temperature over 15 ps, followed by a second NPT step in which the temperature was maintained for an additional 35 ps to ensure full relaxation of the structure. Once the system was equilibrated at the target temperature, plain time integration was conducted for 400 ps. During this period, the system heat flux (J) was recorded every 10 steps as part of the equilibrium molecular dynamics (EMD) simulation.

The thermal conductivity κ was calculated from the recorded heat flux data using the Green-Kubo formalism [24,25], which provides bulk-limit values due to the use of periodic boundary conditions. Details of how we calculate κ from the heat flux data can be found in our previous work [26]. To account for statistical uncertainties inherent in the Green-Kubo approach, three independent simulations were performed, each with a distinct initial random velocity distribution. The κ values reported in this study represent the average of these three independent simulations, ensuring robust and reliable results.

2.3. Nonequilibrium molecular dynamics

Nonequilibrium molecular dynamics (NEMD) simulations are employed to investigate the dependence of κ of PEEK in the cross-chain direction as a function of the number of chains (i.e., the thickness of PEEK in the cross-chain direction). To achieve this, bulk PEEK supercells with varying numbers of chains stacked along the y direction are simulated. The cross-sectional dimensions of the PEEK supercells are fixed at 2×4 unit cells along the x and z directions, respectively.

In the NEMD simulations, the supercell is placed between hot and cold baths, each containing 16 layers of chains along the y direction. Following a structural relaxation process similar to that used in the EMD simulations described earlier, two layers of chains at both ends of the system are frozen, mimicking fixed boundary conditions. This ensures structural stability and prevents heat flow across the domain boundaries in the y direction. Subsequently, plain time integration is performed in LAMMPS, during which Nosé-Hoover thermostats actively

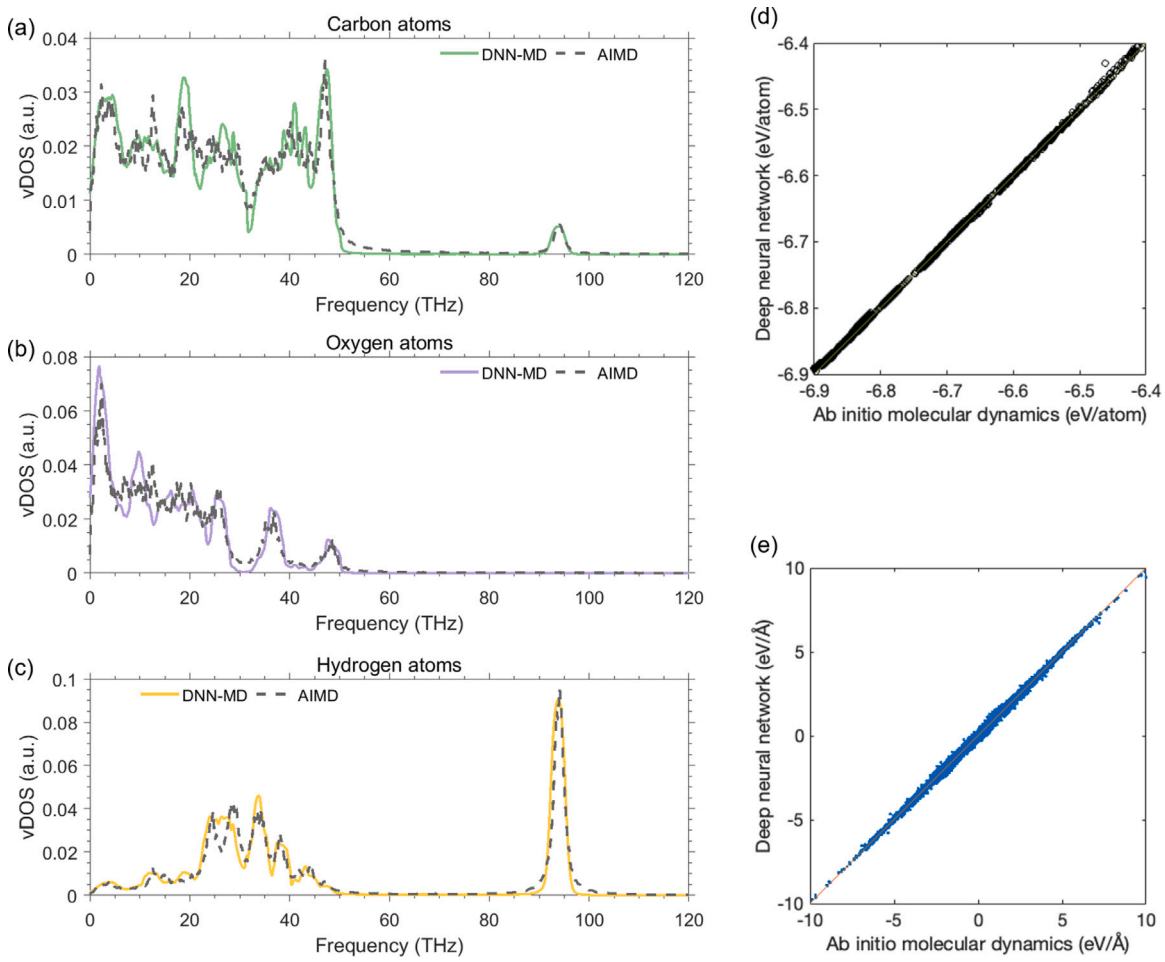

Fig. 2. Validation of the DNN potential against AIMD data. (a)–(c) The vibrational density of states of bulk PEEK predicted by AIMD and DNN based MD simulations for (a) carbon, (b) oxygen, and (c) hydrogen atoms. (d) and (e) The comparison between the DNN and AIMD predictions of (d) energies and (e) forces.

rescale atomic velocities to maintain the temperatures of the hot and cold baths at 315 K and 285 K, respectively. As a result, heat flows from the hot bath to the cold bath across the PEEK supercell along the y direction. This process continues for 1500 ps to establish steady-state heat conduction.

The apparent κ of the PEEK supercell is then determined from the steady-state heat current and the corresponding temperature gradient, based on Fourier's law, following a procedure similar to that described in our previous study [27].

2.4. Model systems

In this work, we study single-chain PEEK, bulk crystalline PEEK, and amorphous PEEK. The single-chain and bulk crystalline structures are readily built by replicating the corresponding unit cell along the chain direction (for single-chain PEEK) or along all three dimensions (for bulk PEEK), while the amorphous PEEK is obtained through a melt-quenching process. Although polymer chains in bulk PEEK can theoretically adopt different stacking configurations, it is well established that the staggered stacking order is the most stable phase in bulk crystalline PEEK. This is further corroborated by our MD simulations, where bulk PEEK with an initially aligned stacking order transitioned to the staggered stacking order during the simulation. Nevertheless, it is worth noting that stacking order can significantly impact the thermal transport properties of 2D vdW materials, such as graphite, hexagonal boron nitride, and other 2D compounds composed of heavy elements [28–30].

In order to generate amorphous PEEK, we leave gaps along chain direction and raise the system temperature to 700 K in the canonical ensemble (NVT ensemble) to intentionally melt those chains and enable them entangle with each other. Subsequently, we use NPT to relax the previous melting PEEK along chain direction to get rid of the gaps. Finally, we decrease the system temperature from 700 K to target temperatures (300 K, 400 K, 500 K, and 600 K) and then output the heat flux information in plain time integration to calculate corresponding temperature-dependent κ. Especially, different time durations (7.5 ps, 15 ps, and 30 ps) are employed when cooling the system temperature from 700 K to target temperature to generate three different amorphous PEEK structures.

Fig. 3a presents snapshots of the melt-quenching process, which starts with a bulk crystalline structure and results in an amorphous structure characterized by entangled chains extending in all three dimensions. As depicted in Fig. 3b, the radial distribution functions (RDFs) for single-chain, crystalline, and amorphous bulk PEEK are similar, indicating the preservation of polymer chain integrity in both the crystalline and amorphous bulk structures obtained in this study.

Furthermore, Fig. 3c illustrates the vDOS for the three types of PEEK structures calculated from our EMD simulations based on the DNN potential. Notably, the vDOS of bulk crystalline and bulk amorphous PEEK are similar, reinforcing our conclusion that the chains in the amorphous phase maintain their integrity, akin to those in the crystalline phase, but are merely twisted and entangled. Conversely, the vDOS of single-chain PEEK exhibits sharper peaks compared to the bulk phases, indicating a significant influence of interchain interactions on the vibrational properties of polymer chains.

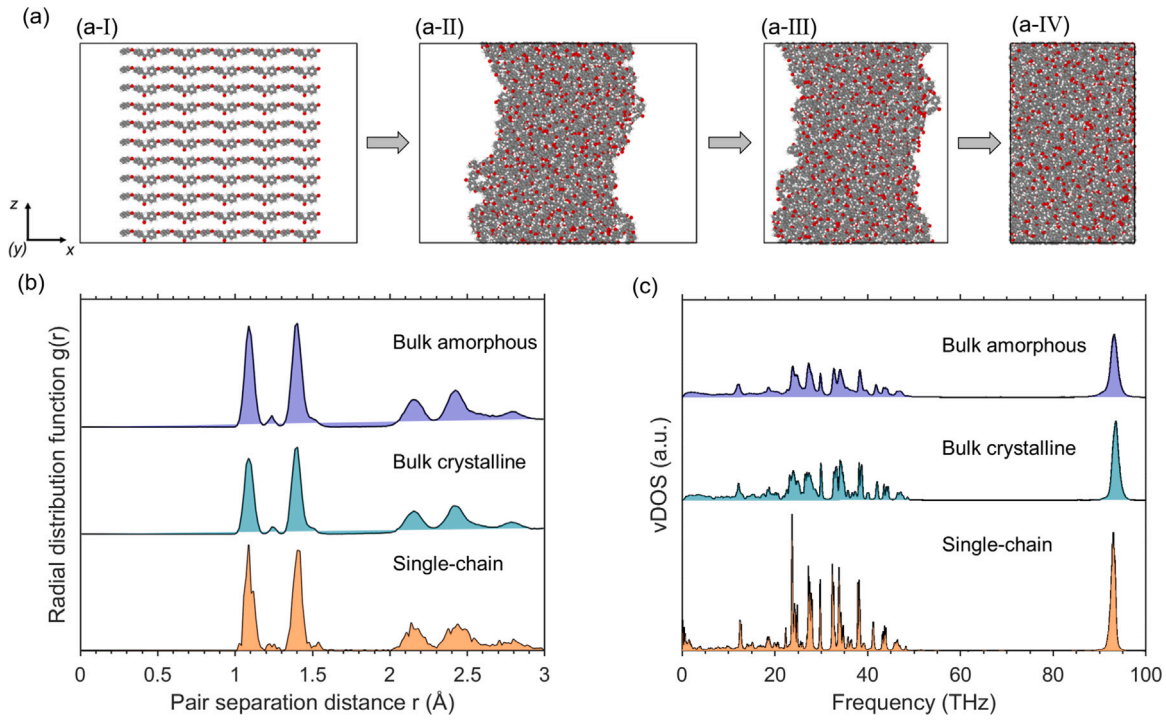

Fig. 3. (a) Illustrations of obtaining the amorphous PEEK by (a-I) generating a bulk PEEK with gaps along x direction, (a-II) melting the bulk PEEK at 700 K, where chains well entangle with each other, (a-III) gradually squeezing the gaps by applying pressure along x direction at 700 K, and (a-IV) quenching the melting PEEK from 700 K to lower temperatures. (b) Radial distribution function and (c) vDOS of single-chain, bulk crystalline, and amorphous PEEK structures predicted by EMD simulations using the DNN potential.

2.5. Spectral energy density analysis

The phonon spectral energy density (SED) analysis evaluates the kinetic energy of different phonon modes, revealing essential phonon properties such as phonon dispersion relations, phonon group velocities, and phonon lifetimes at finite temperatures for various structures [31–33]. It is defined in terms of the time-domain normal mode coordinates $q_{k,v}(t)$, as [31]

$$q_{\boldsymbol{k},v}(t) = \sum_{\alpha}^{3}\sum_{b}^{n}\sum_{l}^{N_c}\sqrt{\frac{m_b}{N_c}}u_{\alpha}^{l,b}(t)e_{b,\alpha}^{\boldsymbol{k},v*}exp[i\boldsymbol{k}\cdot\boldsymbol{r}_0^l], \tag{1}$$

where $u_{\alpha}^{l,b}(t)$ represents the αth component of the displacement of bth basis atom in the lth unit cell, m_b is atomic mass, N_c is the total number of primitive unit cells of the entire system, t is time, $\boldsymbol{k}$ denotes wave vector, v is phonon polarization, and $\boldsymbol{r}_0$ is the equilibrium position of each unit cell. $q_{\boldsymbol{k},v}(t)$ data are collected from the NVE ensemble of EMD simulations over a duration of 200 ps, ensuring a high resolution of 0.005 THz for accurate analysis of phonon properties in the frequency domain. Subsequently, SED is calculated through Fourier transform ($\mathcal{F}[\cdot]$) of the time derivative of $q_{\boldsymbol{k},v}(t)$ as [31]

$$\boldsymbol{\Phi}_{\boldsymbol{k},v}(\omega) = |\mathcal{F}[\dot{q}_{\boldsymbol{k},v}(t)]|^2 = \frac{\boldsymbol{C}_{\boldsymbol{k},v}}{(\omega-\omega_{\boldsymbol{k},v}^{A})^2+(\tau_{\boldsymbol{k},v}^{-1})^2/4}, \tag{2}$$

where $\boldsymbol{\Phi}_{\boldsymbol{k},v}(\omega)$ is the SED, ω is the angular frequency, and C is a constant. The transformed data is fitted with the Lorentzian function to obtain the peak position $\omega_{\boldsymbol{k},v}^{A}$ and phonon lifetime ($\tau_{\boldsymbol{k},v}$).

3. Results and discussions

3.1. A comparison between single-chain and bulk PEEK

Fig. 4 shows the κ of PEEK in different phases as a function of temperature. Notably, the in-chain κ of single-chain PEEK is on the order of 10 W/m-K and decreases with increasing temperature. This trend is attributed to increased anharmonic phonon scattering, a well-known phenomenon in materials where phonons are the primary heat carriers [34]. Similarly, the in-chain κ of bulk crystalline PEEK also decreases significantly with temperature due to enhanced anharmonic scattering. In contrast, the κ of amorphous PEEK and the cross-chain κ of bulk crystalline PEEK remain relatively independent of temperature. In the following sections of this paper, we will elucidate the mechanisms for the differences in κ values among these various PEEK structures.

It is well understood theoretically, from MD simulations and first-principles calculations, that the κ of single-chain polymers is usually much higher than that of their bulk counterparts [16,35–37]. This is due to significant interchain interactions that cause extensive anharmonic phonon scattering, which reduces the κ of phonon modes traveling along each chain. As shown in Fig. 4a and b, the κ of single-chain PEEK is approximately 14.6 W/m-K at 300 K, while the κ of bulk crystalline PEEK along the chain direction is only 3.4 W/m-K. This aligns with previous findings on polyethylene, polyvinylidene fluoride (PVDF), and other polymers, all of which demonstrate an order-of-magnitude lower κ in bulk form compared to their single-chain counterparts [16,35–37], highlighting the significant impact of chain-chain interactions on phonon scattering.

To better understand the underlying mechanism behind the significantly lower κ of bulk crystalline PEEK compared to its single-chain counterpart, we perform SED analysis on both structures to examine their phonon dispersion relations and phonon lifetimes (that is, the inverse of the scattering rates).

Fig. 5a and b display the SED heat maps in frequency-wavevector coordinates, where the color represents SED energy intensity. Several acoustic branches are clearly visible on the heat maps, with the lowest branch corresponding to a transverse acoustic (TA) phonon branch. Evidently, the slope of this TA branch significantly decreases from the single-chain structure (panel a) to the bulk crystalline structure (panel b). This flattening of the TA branch indicates significantly reduced group velocities for these phonon modes, thereby reducing their contribution to thermal transport. Additionally, as shown in Fig. 5d and e, the

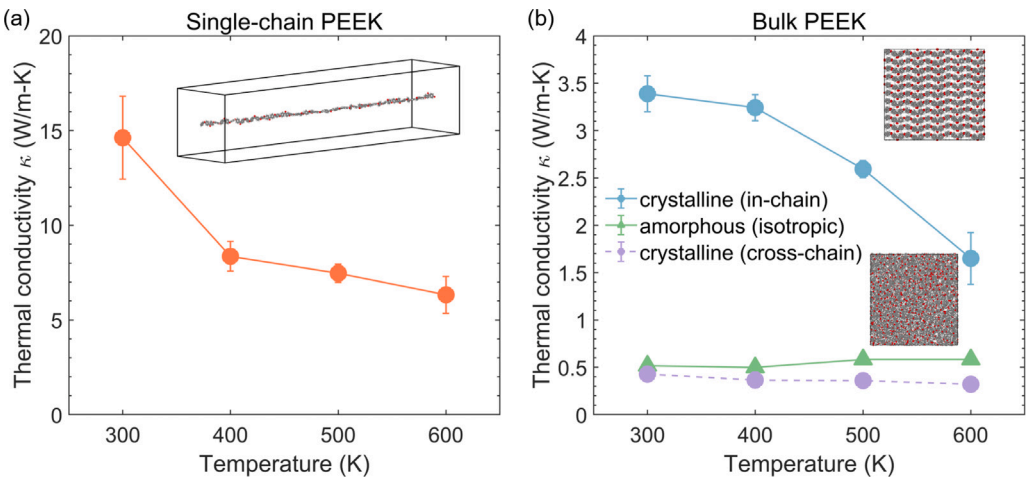

Fig. 4. Illustrations of temperature-dependent (a) in-chain κ of single-chain PEEK, (b) both in-chain κ (blue circular symbols with solid line) and cross-chain κ (purple circular symbols with dashed line) of bulk crystalline PEEK, and isotropic κ of bulk amorphous PEEK (green triangular symbols with solid line).

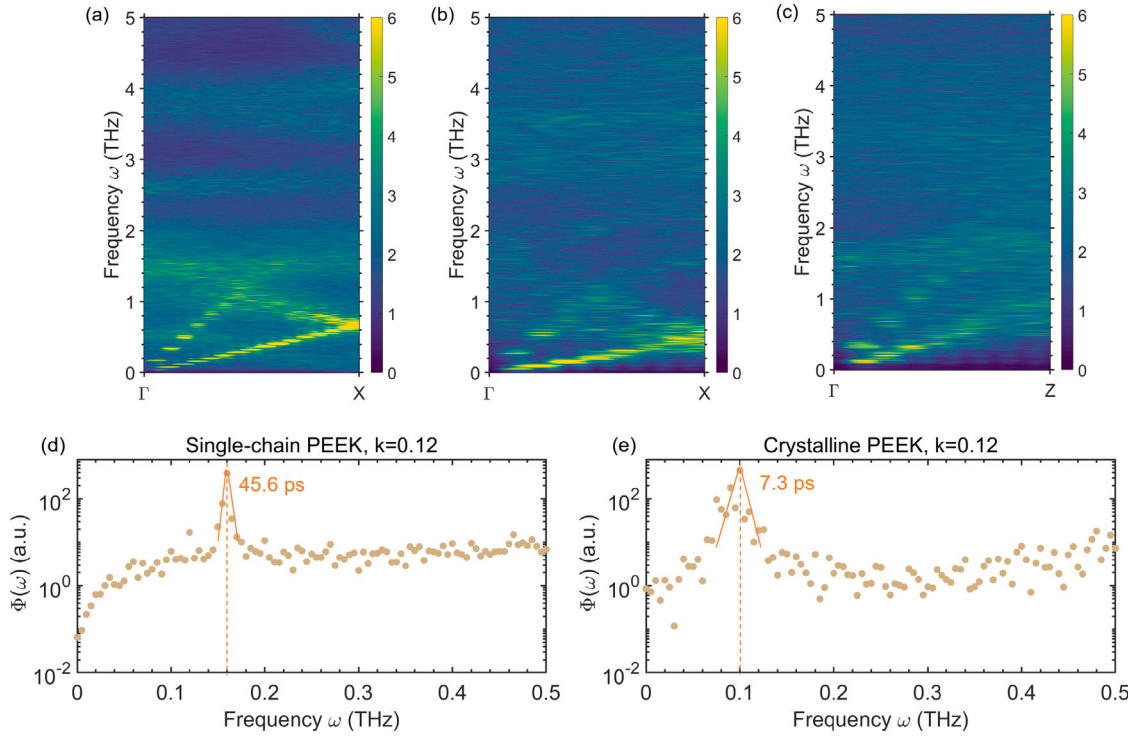

Fig. 5. Comparison of SED contours of (a) single-chain PEEK along in-chain direction [1 0 0], (b) bulk PEEK along in-chain direction [1 0 0], and (c) bulk PEEK along cross-chain direction [0 0 1] over 200 ps at 300 K within [0 5 THz]. Semilogarithmic plot of the SED magnitude along in-chain direction at 300 K with k = 0.12 for frequency below 0.5 THz: (d) single-chain PEEK and (e) crystalline PEEK.

TA phonon mode in single-chain PEEK has a much longer lifetime (45.6 ps) than in bulk PEEK (7.3 ps). The comparison of phonon lifetimes for more k points can be found in Fig. S2 of Supplementary Materials. Based on these results, we conclude that bundling single-chain PEEK into a bulk polymer reduces κ through the flattening of the TA phonon branch and increased phonon scattering due to interchain interactions.

3.2. Thermal transport in amorphous PEEK

In practical applications, such as 3D printing, PEEK is typically utilized in an amorphous state, where the polymer chains are entangled and twisted. To account for this characteristic, we generate amorphous PEEK structures from the crystalline state through a melt-quenching process, as illustrated in Fig. 3a.

The κ of melt-quenched PEEK, as shown in Fig. 4b, is significantly lower than the in-chain κ of its crystalline counterpart but slightly higher than its cross-chain κ. This behavior arises because, in amorphous PEEK, phonons often travel across chains, where heat conduction is less efficient than within individual chains. Within PEEK chains, covalent bonds facilitate efficient phonon transport, while interchain regions rely on weaker vdW interactions, as evidenced by the markedly lower cross-chain κ compared to the in-chain κ of crystalline PEEK, as shown in Fig. 4b.

Even for phonons traveling within the chains of amorphous PEEK, the effective κ is reduced due to the twisted and disordered trans-

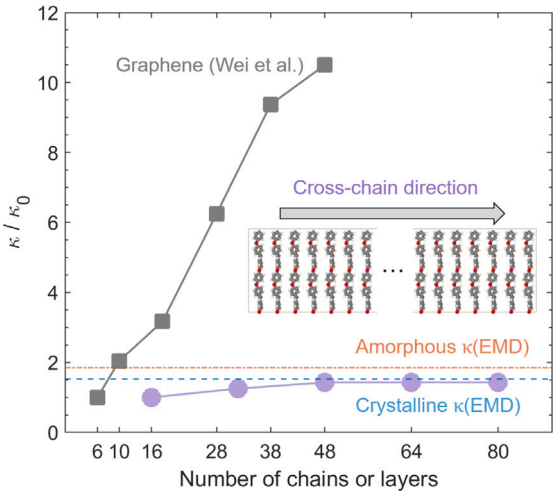

Fig. 6. Room-temperature κ/κ_0 of PEEK or multilayer graphene as a function of the number of chains or layers in the cross-chain or cross-plane direction, where κ_0 is the κ of smallest number of chains or layers. Purple circular symbols represent the values predicted by NEMD simulations. The blue dashed line indicates the bulk-limit value of crystalline PEEK, while the red dash-dotted line corresponds to the bulk-limit value of amorphous PEEK. Gray square symbols refer to the values of multilayer graphene by Wei et al. [38] from NEMD simulations.

port pathways. The physics underlying cross-chain phonon thermal transport will be discussed in greater detail later in this paper.

3.3. Thermal transport across chains

VdW materials have garnered significant attention in recent years due to their unique electronic and photonic properties. In terms of thermal transport, it has been observed in graphite and multilayer graphene that their κ increases notably with the number of layers, indicating strong ballistic phonon transport behavior [38]. Recognizing that interchain interactions are also governed by vdW interactions and that the impact of the number of chains on thermal transport across chains has not been previously studied, we perform NEMD simulations to investigate the dependence of κ in the cross-chain direction on the number of chains.

As shown in Fig. 6, the cross-chain κ of PEEK increases with the number of chains (or layers of chains) up to 48 chains, after which κ becomes constant. Notably, the κ of multilayer PEEK increases with the number of vdW-bonded layers, resembling the increasing cross-plane κ of multilayer graphene and other materials. However, unlike graphene, the dependence of PEEK's cross-chain κ on the number of chains is much weaker than the dependence of multilayer graphene's cross-plane κ on the number of layers.

This behavior arises from the significant coupling between intrachain phonons (within individual polymer chains) and interchain phonons (between adjacent chains) in PEEK. This coupling is markedly stronger than the coupling observed between intralayer phonons (within individual graphene layers) and interlayer phonons (between layers) in multilayer graphene. The weak coupling in multilayer graphene is evidenced by the similar in-plane κ values of multilayer graphene (or graphite) and single-layer graphene. In contrast, as demonstrated in this study for PEEK and reported for other polymers such as polyethylene, the in-chain κ of bulk polymers is often an order of magnitude lower than that of their single-chain counterparts. This disparity indicates that the intrachain phonon–interchain phonon interactions in PEEK are sufficiently strong to significantly impede the transport of intrachain phonons. Conversely, these robust interchain interactions can also hinder the transport of interchain phonons, thereby diminishing the dependence of PEEK's cross-chain κ on the number of chains. Further evidence of the strong interchain coupling in PEEK is provided by the pronounced slope of the phonon acoustic branches in the cross-chain direction, as shown in Fig. 5c, which reflects the presence of stiff bonding between chains.

4. Conclusion

In this work, we trained a DNN interatomic potential from AIMD simulations for PEEK, a crucial material in modern industry that is compatible with 3D printing. We found that the in-chain κ of bulk crystalline PEEK is much lower than that of its single-chain counterpart. This reduction is due to significant interchain interactions that increase phonon scattering and reduce the phonon group velocities of TA phonons. Additionally, we found that the cross-chain κ of PEEK increases with the number of chains in the heat transfer direction, indicating some degree of ballistic phonon transport across the chain. However, the dependence of cross-chain κ on the number of chains is relatively weak, unlike the case of multilayer 2D materials, where the cross-plane κ increases significantly with the number of layers. This is because of the strong coupling between interchain and intrachain phonons in PEEK, which scatters interchain phonons and reduces the ballistic nature of cross-chain thermal transport. Finally, our simulations on amorphous PEEK show a κ that is similar to, though slightly higher than, the cross-chain κ of PEEK, indicating that thermal transport in amorphous PEEK is governed by cross-chain thermal transport due to the significantly entangled chains. This work will be useful for the understanding of thermal transport behaviors in PEEK and for its application in 3D printing or other fields.

CRediT authorship contribution statement

Haoran Cui: Writing – review & editing, Writing – original draft, Visualization, Software, Methodology, Investigation, Formal analysis, Data curation. **Weijian Hua:** Writing – review & editing, Writing – original draft, Investigation, Formal analysis, Data curation. **Lei Cao:** Writing – review & editing, Writing – original draft, Investigation. **Yifei Jin:** Writing – review & editing, Writing – original draft, Supervision, Methodology, Investigation, Funding acquisition, Formal analysis, Conceptualization. **Yan Wang:** Writing – review & editing, Writing – original draft, Supervision, Project administration, Methodology, Investigation, Funding acquisition, Formal analysis, Conceptualization.

Declaration of competing interest

The authors declare the following financial interests/personal relationships which may be considered as potential competing interests: Yan Wang reports financial support was provided by National Science Foundation. If there are other authors, they declare that they have no known competing financial interests or personal relationships that could have appeared to influence the work reported in this paper.

Acknowledgments

Cui and Wang acknowledge the financial support from the National Science Foundation, United States (CBET-2211696). Hua and Jin acknowledge the financial support from the National Science Foundation, United States (OIA-2229004). The authors acknowledge the support of Research and Innovation and the Cyberinfrastructure Team in the Office of Information Technology at the University of Nevada, Reno, for facilitation and access to the Pronghorn High-Performance Computing Cluster.

Appendix A. Supplementary data

Supplementary material related to this article can be found online at https://doi.org/10.1016/j.commatsci.2024.113641.

Data availability

The data that support the findings of this study are available from the corresponding authors upon reasonable request.

References

[1] D.P Jones, D.C Leach, D.R. Moore, Mechanical properties of poly(ether-ether-ketone) for engineering applications, Polymer 26 (9) (1985) 1385–1393, Speciality Polymers 84.

[2] D Garcia-Gonzalez, A Rusinek, T Jankowiak, A. Arias, Mechanical impact behavior of polyether–ether–ketone (peek), Compos. Struct. 124 (2015) 88–99.

[3] João da Silva Burgal, Ludmila G. Peeva, Santosh Kumbharkar, Andrew Livingston, Organic solvent resistant poly(ether-ether-ketone) nanofiltration membranes, J. Membr. Sci. 479 (2015) 105–116.

[4] Ning Cao, Yirong Sun, Jin Wang, Haibo Zhang, Jinhui Pang, Zhenhua Jiang, Strong acid- and solvent-resistant polyether ether ketone separation membranes with adjustable pores, Chem. Eng. J. 386 (2020) 124086.

[5] Youngchul Lee, Roger S. Porter, Effects of thermal history on crystallization of poly (ether ether ketone)(peek), Macromolecules 21 (9) (1988) 2770–2776.

[6] Dan Li, Dingqin Shi, Kai Feng, Xianfeng Li, Huamin Zhang, Poly (ether ether ketone) (peek) porous membranes with super high thermal stability and high rate capability for lithium-ion batteries, J. Membr. Sci. 530 (2017) 125–131.

[7] B.J Briscoe, B.H Stuart, S Sebastian, P.J. Tweedale, The failure of poly (ether ether ketone) in high speed contacts, Wear 162–164 (1993) 407–417, Wear of Materials: Proceedings of the 9th International Conference.

[8] J. Paulo Davim, Pedro Reis, Machinability study on composite (polyetheretherketone reinforced with 30% glass fibre–peek gf 30) using polycrystalline diamond (pcd) and cemented carbide (k20) tools, Int. J. Adv. Manuf. Technol. 23 (2004) 412–418.

[9] H.M Li, R.A Fouracre, M.J Given, H.M Banford, S Wysocki, S. Karolczak, The effects on polyetheretherketone and polyethersulfone of electron and/spl gamma/irradiation, IEEE Trans. Dielectr. Electr. Insul. 6 (3) (1999) 295–303.

[10] Cong Wang, J Ma, Wen Cheng, Formation of polyetheretherketone polymer coating by electrophoretic deposition method, Surf. Coat. Technol. 173 (2) (2003) 271–275.

[11] Emine Feyza Sukur, Thermally conditioned aerospace-grade carbon fiber reinforced polyether ketone ketone composites: structure, impact response, and thermomechanical performance, Polym. Compos. 44 (4) (2023) 2530–2544.

[12] G Zhang, W.-Y Li, M Cherigui, C Zhang, H Liao, J.-M Bordes, C. Coddet, Structures and tribological performances of peek (poly-ether-ether-ketone)-based coatings designed for tribological application, Prog. Org. Coat. 60 (1) (2007) 39–44.

[13] Nathan T. Evans, F Brennan Torstrick, Christopher S.D. Lee, Kenneth M. Dupont, David L. Safranski, W Allen Chang, Annie E. Macedo, Angela S.P. Lin, Jennifer M. Boothby, Daniel C. Whittingslow, Robert A. Carson, Robert E. Guldberg, Ken Gall, High-strength, surface-porous polyether-ether-ketone for load-bearing orthopedic implants, Acta Biomater. 13 (2015) 159–167.

[14] Ivan Vladislavov Panayotov, Valérie Orti, Frédéric Cuisinier, Jacques Yachouh, Polyetheretherketone (peek) for medical applications, J. Mater. Sci., Mater. Med. 27 (2016) 1–11.

[15] Sunpreet Singh, Chander Prakash, Seeram Ramakrishna, 3D printing of polyether-ether-ketone for biomedical applications, Eur. Polym. J. 114 (2019) 234–248.

[16] Asegun Henry, Gang Chen, High thermal conductivity of single polyethylene chains using molecular dynamics simulations, Phys. Rev. Lett. 101 (2008) 235502.

[17] Tengfei Ma, Yan Wang, Giant reduction in thermal conductivity of single-chain polyvinylidene fluoride (pvdf) under external tensile strain, Phys. Chem. Chem. Phys. 24 (18) (2022) 11315–11321.

[18] Teng Zhang, Tengfei Luo, Role of chain morphology and stiffness in thermal conductivity of amorphous polymers, J. Phys. Chem. B 120 (4) (2016) 803–812.

[19] Han Wang, Linfeng Zhang, Jiequn Han, E. Weinan, Deepmd-kit: A deep learning package for many-body potential energy representation and molecular dynamics, Comput. Phys. Comm. 228 (2018) 178–184.

[20] Yuzhi Zhang, Haidi Wang, Weijie Chen, Jinzhe Zeng, Linfeng Zhang, Han Wang, E. Weinan, Dp-gen: A concurrent learning platform for the generation of reliable deep learning based potential energy models, Comput. Phys. Comm. 253 (2020) 107206.

[21] Aidan P Thompson, H. Metin Aktulga, Richard Berger, Dan S Bolintineanu, W. Michael Brown, Paul S Crozier, Pieter J. in't Veld, Axel Kohlmeyer, Stan G Moore, Trung Dac Nguyen, et al., Lammps-a flexible simulation tool for particle-based materials modeling at the atomic, meso, and continuum scales, Comput. Phys. Comm. 271 (2022) 108171.

[22] Shuichi Nosé, A unified formulation of the constant temperature molecular dynamics methods, J. Chem. Phys. 81 (1) (1984) 511–519.

[23] William G. Hoover, Canonical dynamics: Equilibrium phase-space distributions, Phys. Rev. A 31 (3) (1985) 1695.

[24] Melville S. Green, Markoff random processes and the statistical mechanics of time-dependent phenomena, ii. irreversible processes in fluids, J. Chem. Phys. 22 (3) (1954) 398–413.

[25] Ryogo Kubo, Statistical–mechanical theory of irreversible processes, i. general theory and simple applications to magnetic and conduction problems, J. Phys. Soc. Jpn. 12 (6) (1957) 570–586.

[26] Yan Wang, Chongjie Gu, Xiulin Ruan, Optimization of the random multilayer structure to break the random-alloy limit of thermal conductivity, Appl. Phys. Lett. 106 (7) (2015).

[27] Haoran Cui, Tengfei Ma, Yan Wang, Elucidating optimal nanohole structures for suppressing phonon transport in nanomeshes, 2D Mater. 11 (3) (2024) 035026.

[28] Masoud H. Khadem, Aaron P. Wemhoff, Molecular dynamics predictions of the influence of graphite stacking arrangement on the thermal conductivity tensor, Chem. Phys. Lett. 574 (2013) 78–82.

[29] Hao Wu, Yi-Lin Zhang, Zhi-Xin Guo, Xin-Gao Gong, Anomalous high thermal conductivity in heavy element compounds with van der waals interaction, Appl. Phys. Lett. 121 (18) (2022).

[30] S.G Wang, H.F Feng, Zhi-Xin Guo, Stacking and thickness effects on cross-plane thermal conductivity of hexagonal boron nitride, Comput. Mater. Sci. 228 (2023) 112345.

[31] John A. Thomas, Ryan M. Iutzi, Alan J.H. McGaughey, Thermal conductivity and phonon transport in empty and water-filled carbon nanotubes, Phys. Rev. B 81 (2010) 045413.

[32] Iyyappa Rajan Panneerselvam, Haoran Cui, Theodore Maranets, Yan Wang, Disorder-dominated and scattering-dominated thermal transport in clathrate hydrates, Comput. Mater. Sci. 244 (2024) 113189.

[33] Haoran Cui, Theodore Maranets, Tengfei Ma, Yan Wang, Spectral analysis of coherent and incoherent phonon transport in silicon nanomeshes, Phys. Rev. B 110 (2024) 075301.

[34] Tengfei Ma, Pranay Chakraborty, Xixi Guo, Lei Cao, Yan Wang, First-principles modeling of thermal transport in materials: Achievements, opportunities, and challenges, Int. J. Thermophys. 41 (2020) 1–37.

[35] Sheng Shen, Asegun Henry, Jonathan Tong, Ruiting Zheng, Gang Chen, Polyethylene nanofibres with very high thermal conductivities, Nature Nanotechnol. 5 (4) (2010) 251–255.

[36] Xinjiang Wang, Massoud Kaviany, Baoling Huang, Phonon coupling and transport in individual polyethylene chains: a comparison study with the bulk crystal, Nanoscale 9 (45) (2017) 18022–18031.

[37] Tengfei Ma, Yan Wang, Giant reduction in thermal conductivity of single-chain polyvinylidene fluoride (pvdf) under external tensile strain, Phys. Chem. Chem. Phys. 24 (18) (2022) 11315–11321.

[38] Zhiyong Wei, Zhonghua Ni, Kedong Bi, Minhua Chen, Yunfei Chen, Interfacial thermal resistance in multilayer graphene structures, Phys. Lett. A 375 (8) (2011) 1195–1199.